Optimal performance of reciprocating demagnetization quantum refrigerators

Ronnie Kosloff and Tova Feldmann
Institute of Chemistry, The Hebrew University, Jerusalem 91904, Israel
(Received 1 January 2010; published 23 July 2010)

A reciprocating quantum refrigerator is studied with the purpose of determining the limitations of cooling to absolute zero. The cycle is based on demagnetization and magnetization of a working medium. We find that if the energy spectrum of the working medium possesses an uncontrollable gap, and in addition there is noise on the controls, then there is a minimum achievable temperature above zero. The reason is that even a negligible amount of noise prevents adiabatic following during the demagnetization stage. This results with a minimum temperature, $T_c(\min)>0$, which scales with the energy gap. The refrigerator is based on an Otto cycle where the working medium is an interacting spin system with an energy gap. For this system the external control Hamiltonian does not commute with the internal interaction. As a result during the demagnetization and magnetization segments of the operating cycle the system cannot follow adiabatically the temporal change in the energy levels. We connect the nonadiabatic dynamics to quantum friction. An adiabatic measure is defined characterizing the rate of change of the Hamiltonian. Closed-form solutions are found for a constant adiabatic measure for all the cycle segments. We have identified a family of quantized frictionless cycles with increasing cycle times. These cycles minimize the entropy production. Such frictionless cycles are able to cool to $T_c=0$. External noise on the controls eliminates these frictionless cycles. The influence of phase and amplitude noise on the demagnetization and magnetization segments is explicitly derived. An extensive numerical study of optimal cooling cycles was carried out which showed that at sufficiently low temperature the noise always dominated restricting the minimum temperature.

DOI: 10.1103/PhysRevE.82.011134 PACS number(s): 05.70.Ln, 03.65.Yz, 07.20.Pe

I. INTRODUCTION

Quantum thermodynamics is devoted to the study of thermodynamical processes within the context of quantum dynamics. The thermodynamic tradition of learning by example is translated to establishing quantum analogs of heat engines. These studies unravel the intimate connection between the laws of thermodynamics and their quantum origins [1–22]. In this tradition the present study is directed toward the quantum study of the third law of thermodynamics [23–26], in particular the unattainability principle [27,28]: is it possible to cool a system as close as we desire to the absolute zero $T_c=0$ or alternatively cooling stops at some finite temperature $T_c>0$? The present study addresses this issue based on a four-stroke reciprocating quantum refrigerator.

Reciprocating refrigerators operate by a working medium shuttling heat from the cold to the hot reservoir. The task is carried out by a controlled dynamical system. A change in the Hamiltonian of the system is accompanied by a change in the internal energy. Upon contact with the cold side the internal energy of the working medium is forced to be lower than the equilibrium energy at T_c—the cold bath temperature. Only under these conditions heat will flow from the cold bath to the working medium. A reciprocal relation is required on the hot side. Explicitly a quantum refrigerator is studied where the control of temperature is governed by manipulating the energy levels of the system.

The main issues to be addressed are

(i) What are the restrictions imposed by the working medium?

(ii) What are the conditions for optimizing the cooling power when $T_c\rightarrow 0$?

(iii) Is there a minimum temperature above the absolute zero?

To gain insight on these issues a reverse Otto cycle is considered where the working medium consists of interacting spin system. The magnetization and demagnetization stages are carried out by varying an external magnetic field which alters the energy levels of the working medium. Such a model is a simplified version of adiabatic demagnetization refrigerator (ADR) [29–31]. These refrigerators have found not only use in cooling detectors to very low temperatures in space missions but also in an attempt to replace the existing technology in home appliances [32–34].

The present paper is a comprehensive account of a quantum refrigerator following a brief report [35]. The approach is based on the analysis of quantum dynamical thermodynamical observables. It is in the spirit of a series of studies on first-principles four-stroke quantum engines operating in finite time [36–44]. These studies established that the model engines display the irreversible characteristics of common finite-power engines [45].

The key to the performance is the working medium. A quantum working medium possesses a Hamiltonian that can be controlled externally. Typically external control influences only part of the Hamiltonian operator,

$$\hat{\mathbf{H}} = \hat{\mathbf{H}}_{int} + \hat{\mathbf{H}}_{ext}(\omega), \tag{1}$$

where $\hat{\mathbf{H}}_{int}$ is the internal part of the Hamiltonian which is responsible for the irreducible gap in the energy spectrum. $\hat{\mathbf{H}}_{ext}(\omega)$ is the control Hamiltonian where $\omega=\omega(t)$ is the time-dependent external control field. Generically, the internal and external parts do not commute $[\hat{\mathbf{H}}_{int},\hat{\mathbf{H}}_{ext}]\neq 0$. This has a profound effect on the adiabatic segments of the refrigerator since then $[\hat{\mathbf{H}}(t),\hat{\mathbf{H}}(t')]\neq 0$. A state which was initially pre-

pared to be diagonal in the temporary energy eigenstates cannot follow adiabatically the changes in energy levels induced by the control. The result is an additional power required to execute the adiabatic segment termed quantum friction [40]. This friction has been found to limit the performance of the heat engines [41–44]. In quantum refrigerators the frictional heating in the expansion-demagnetization segment limits the minimal temperature of the working medium. This in turn puts a restriction on the minimum temperature of the bath that heat can be extracted from. This means that a refrigerator that can pump heat up to the absolute zero has to be frictionless.

A good characterization of the deviation from adiabaticity is the difference between the von Neumann entropy of the state $\mathcal{S}_{vn}=-\mathrm{tr}\{\hat{\boldsymbol{\rho}}\ln\hat{\boldsymbol{\rho}}\}$ and the energy entropy defined by the projections on the energy eigenstate $\mathcal{S}_E=-\Sigma p_j \ln p_j$, where p_j is the population of energy state j. Equality is obtained only for perfect adiabatic following, $[\hat{\mathbf{H}}(t),\hat{\mathbf{H}}(t')]=0$ [41].

One obvious solution to a frictionless operation is perfect adiabatic following i.e., at each time the system is diagonal in the temporary energy eigenstates. The drawback of such an approach is that it requires ever increasing time to execute this move when the temperature of the cold bath approaches $T_c=0$. Demanding that only at the initial and final times the system is diagonal in the energy representation leads to additional opportunities for frictionless solutions. For a working medium consisting of harmonic oscillators such solutions have been found [46,47] which are characterized by a fast finite expansion time. If negative frequencies are permissible, this time can be reduced further [48]. For these models where the energy gap can be controlled to follow the cold bath temperature T_c, the absolute zero seems attainable.

The present study explores a different working medium which possesses an uncontrollable finite gap in the energy-level spectrum between the ground and first excited states. We find that the absolute zero temperature is unattainable due to noise in the control. The essentials of the refrigerator cycle are described in Sec. II. In Sec. III a family of frictionless solutions for this cycle is developed. These solutions also serve as a basis to study the influence of noise on the controls described in Sec. IV. Our basic finding is that the energy gap combined with unavoidable quantum noise will lead to a finite minimal temperature (Sec. V). In addition we have carried out numerous simulations of refrigeration cycles with linear as well as optimized scheduling of the control $\omega(t)$, leading to a broader understanding of the limitations on cooling (Sec. VI). The summary and conclusions are in Sec. VII. The details of the derivations of optimal adiabatic following and the noise propagator are in the appendixes.

II. THE QUANTUM HEAT PUMP CYCLE OF OPERATION

The working medium in the present study is composed of an interacting spin system. Equation (1) is modeled by the SU(2) algebra of operators. The model is realized by a system of two coupled spins where the internal interaction is described by

$$\hat{\mathbf{H}}_{int}=\tfrac{1}{2}\hbar J(\hat{\boldsymbol{\sigma}}_x^1\otimes\hat{\boldsymbol{\sigma}}_x^2-\hat{\boldsymbol{\sigma}}_y^1\otimes\hat{\boldsymbol{\sigma}}_y^2)\equiv\hbar J\hat{\mathbf{B}}_2, \tag{2}$$

where $\hat{\boldsymbol{\sigma}}$ represents the spin-Pauli operators and J scales the strength of the interparticle interaction. For $J\to 0$, the system approaches a working medium with noninteracting atoms [39]. The external Hamiltonian represents interaction of spins with an external magnetic field,

$$\hat{\mathbf{H}}_{ext}=\tfrac{1}{2}\hbar\omega(t)(\hat{\boldsymbol{\sigma}}_z^1\otimes\hat{\mathbf{I}}^2+\hat{\mathbf{I}}^1\otimes\boldsymbol{\sigma}_z^2)\equiv\omega(t)\hat{\mathbf{B}}_1. \tag{3}$$

The SU(2) is closed with $\hat{\mathbf{B}}_3=\frac{1}{2}(\hat{\boldsymbol{\sigma}}_y^1\otimes\hat{\boldsymbol{\sigma}}_x^2+\hat{\boldsymbol{\sigma}}_x^1\otimes\hat{\boldsymbol{\sigma}}_y^2)$ and $[\hat{\mathbf{B}}_1,\hat{\mathbf{B}}_2]\equiv 2i\hat{\mathbf{B}}_3$.

The total Hamiltonian modeling [Eq. (1)] then becomes

$$\hat{\mathbf{H}}=\hbar(\omega(t)\hat{\mathbf{B}}_1+J\hat{\mathbf{B}}_2). \tag{4}$$

The adiabatic energy levels, the eigenvalues of $\hat{\mathbf{H}}(t)$, are $\epsilon_1=-\hbar\Omega$, $\epsilon_{2/3}=0$, $\epsilon_4=\hbar\Omega$, where $\Omega=\sqrt{\omega^2+J^2}$. For $J\neq 0$ there is a zero-field splitting, an irreducible gap between the ground- and excited-state levels. Equation (4) contains the essential features of the Hamiltonian of magnetic materials [29].

The dynamics of the quantum thermodynamical observables are described by completely positive maps within the formulation of quantum open systems [49–51]. The dynamics is generated by the Liouville superoperator $\mathcal{L}$ studied in the Heisenberg picture,

$$\frac{d\hat{\mathbf{A}}}{dt}=\frac{i}{\hbar}[\hat{\mathbf{H}},\hat{\mathbf{A}}]+\mathcal{L}_D(\hat{\mathbf{A}})+\frac{\partial\hat{\mathbf{A}}}{\partial t}, \tag{5}$$

where $\mathcal{L}_D$ is a generator of a completely positive Liouville superoperator. This formalism allows a reduced description of the working medium, with the environment appearing only implicitly.

The cycle studied is composed of two isomagnetic segments, termed *isochores* where the working medium is in contact with the cold and hot baths and the external control field ω is constant. In addition, there are two segments termed *adiabats* where the external field $\omega(t)$ varies and with it the energy-level structure of the working medium. This cycle is a quantum analog of the Otto cycle [40]. Each segment is characterized by a quantum propagator $\mathcal{U}_s$. The propagator maps the initial state of the working medium to the final state on the relevant segment. The four strokes of the cycle in analogy with the Otto cycle (see Fig. 1) are

(i) *hot isomagnetic (isochore) $A\to B$:* the field is maintained constant $\omega=\omega_h$; the working medium is in contact with the hot bath of temperature T_h. $\mathcal{L}_D$ leads to equilibrium with heat conductance Γ_h, for a period of τ_h. The segment dynamics is described by the propagator $\mathcal{U}_h$.

(ii) *demagnetization (expansion) adiabat $B\to C$:* the field changes from ω_h to ω_c in a time period of τ_{hc}. $\mathcal{L}_D=\mathcal{L}_N$ represents external noise in the controls. The propagator becomes $\mathcal{U}_{hc}$ which is the main subject of study.

(iii) *cold isomagnetic (isochore) $C\to D$:* the field is maintained constant $\omega=\omega_c$; the working medium is in contact with the cold bath of temperature T_c. $\mathcal{L}_D$ leads to equilibrium with heat conductance Γ_c, for a period of τ_c. The segment dynamics is described by the propagator $\mathcal{U}_c$.

(iv) *magnetization (compression) adiabat $D\to A$:* the field changes from ω_c to ω_h in a time period of τ_{ch}; $\mathcal{L}_D=\mathcal{L}_N$ represents external noise in the controls. The propagator becomes $\mathcal{U}_{ch}$.

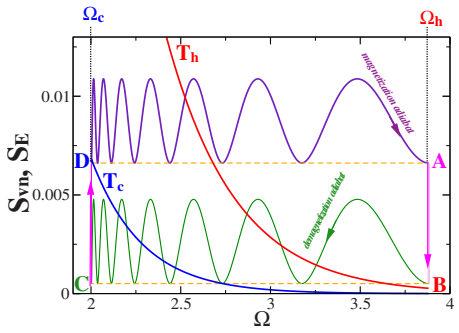

FIG. 1. (Color online) Refrigerator cycle in the frequency entropy plane. The von Neumann entropy $\mathcal{S}_{vn}=-\mathrm{tr}\{\hat{\boldsymbol{\rho}}\ln\hat{\boldsymbol{\rho}}\}$ (*ABCD* rectangle) as well as the energy entropy $\mathcal{S}_E=-\Sigma p_i \ln p_i$ is shown (p_i is the population of energy level i). The hot and cold isotherms $\mathcal{S}_{eq}(T)$ are indicated. On the *adiabats* the energy-level spacings change from $\hbar\Omega_h$ to $\hbar\Omega_c$. The demagnetization *adiabat* and the magnetization *adiabats* revolve by exactly seven periods. The *adiabats* are frictionless since $\mathcal{S}_{vn}=\mathcal{S}_E$ at the beginning and end of the segment. On the *isochores* the energy-level spacing remains constant and the entropy changes due to change in population. The cycle parameters are $\hbar J=2$, $T_c=0.18$, $T_h=0.24$, $\hbar\omega_c=0.1$, $\hbar\omega_h=3.325$, $\tau_c=10.54$, $\tau_h=9.741$, $\tau_{hc}=\tau_{ch}=12.81$, $\mathcal{Q}_c/\tau=2.16\times10^{-5}$, and $\Delta\mathcal{S}^u/\tau=5.4\times10^{-5}$.

The product of the four propagators $\mathcal{U}_s$ is the cycle propagator chosen at point A,

$$\mathcal{U}_{cyc}=\mathcal{U}_{ch}\mathcal{U}_c\mathcal{U}_{hc}\mathcal{U}_h. \tag{6}$$

Eventually, independent of the initial condition, after a few cycles, the working medium will reach a limit cycle characterized as an invariant eigenvector of $\mathcal{U}_{cyc}$ with eigenvalue 1 (one) [42]. The characteristics of the refrigerator are therefore extracted from the limit cycle.

III. QUANTUM THERMODYNAMICAL OBSERVABLES AND THEIR DYNAMICS

To facilitate the study of the dynamics of the cooling cycle, a representation of the state $\hat{\boldsymbol{\rho}}$ and the thermodynamical observables is required. The orthogonal set of time-independent operators $\hat{\mathbf{B}}_\mathbf{i}$ is closed to the dynamics. As a result they can supply a complete vector space to expand the propagators $\mathcal{U}$ and $\hat{\boldsymbol{\rho}}$. A thermodynamically oriented time-dependent vector space which directly addresses the issue of adiabaticity is superior. This set includes the energy $\hat{\mathbf{H}}$ and two additional orthogonal operators:

$$\hat{\mathbf{H}}=\hbar\omega(t)\hat{\mathbf{B}}_\mathbf{1}+\hbar J\hat{\mathbf{B}}_\mathbf{2},\quad \hat{\mathbf{L}}=-\hbar J\hat{\mathbf{B}}_\mathbf{1}+\hbar\omega(t)\hat{\mathbf{B}}_\mathbf{2},$$

$$\hat{\mathbf{C}}=\hbar\Omega(t)\hat{\mathbf{B}}_\mathbf{3}. \tag{7}$$

To uniquely define the state of the system $\hat{\boldsymbol{\rho}}$ the original set is supplemented with two operators: $\hat{\mathbf{V}}=\hbar\Omega\hat{\mathbf{B}}_4=\frac{\hbar}{2}\Omega(\hat{\mathbf{I}}^1\otimes\hat{\boldsymbol{\sigma}}_z^2-\hat{\mathbf{I}}^2\otimes\hat{\boldsymbol{\sigma}}_z^1)$ and $\hat{\mathbf{D}}=\hbar\Omega\hat{\mathbf{B}}_5=\hbar\Omega\hat{\boldsymbol{\sigma}}_z^1\otimes\hat{\sigma}_z^2$. With this operator base the state $\hat{\boldsymbol{\rho}}$ can be expanded as

$$\hat{\boldsymbol{\rho}}=\frac{1}{4}\hat{\mathbf{I}}+\frac{1}{2(\hbar\Omega)^2}\left(\langle\hat{\mathbf{H}}\rangle\hat{\mathbf{H}}+\langle\hat{\mathbf{L}}\rangle\hat{\mathbf{L}}+\langle\hat{\mathbf{C}}\rangle\hat{\mathbf{C}}+\frac{1}{2}\langle\hat{\mathbf{V}}\rangle\hat{\mathbf{V}}+\frac{1}{2}\langle\hat{\mathbf{D}}\rangle\hat{\mathbf{D}}\right), \tag{8}$$

where $\hat{\mathbf{V}}$ and $\hat{\mathbf{D}}$ commute with $\hat{\mathbf{H}}$. The equilibrium value of $\langle\hat{\mathbf{V}}\rangle$ is zero, and once it reaches equilibrium it does not change during the cycle dynamics. As a result the state $\hat{\boldsymbol{\rho}}$ can be described in the energy representation by four expectation values:

$$\hat{\boldsymbol{\rho}}_e=\frac{1}{4}\begin{pmatrix} 1+\frac{1}{\hbar\Omega}(D-2E) & 0 & 0 & \frac{2}{\hbar\Omega}(L+iC) \\ 0 & 1-\frac{1}{\hbar\Omega}D & 0 & 0 \\ 0 & 0 & 1-\frac{1}{\hbar\Omega}D & 0 \\ \frac{2}{\hbar\Omega}(L-iC) & 0 & 0 & 1+\frac{1}{\hbar\Omega}(D+2E) \end{pmatrix}, \tag{9}$$

where $E=\langle\hat{\mathbf{H}}\rangle$, $L=\langle\hat{\mathbf{L}}\rangle$, $C=\langle\hat{\mathbf{C}}\rangle$, and $D=\langle\hat{\mathbf{D}}\rangle$. From Eq. (9) it is clear that when $L=C=0$, $\hat{\boldsymbol{\rho}}_e$ is diagonal in the energy representation, then $[\hat{\boldsymbol{\rho}}(t),\hat{\mathbf{H}}(t)]=0$.

A. Dynamics on the hot and cold isomagnetic segments (*isochores*)

The dynamics on the isomagnetic isochores is dominated by the approach to equilibrium with the hot and cold baths. The equation of motion is derived from Eq. (5) and the Hamiltonian (4), where $\omega(t)$ is constant either ω_h on the hot side or ω_c on the cold side. The dissipative part $\mathcal{L}_D$ has Lindblad's form [49] with parameters chosen to lead to thermal equilibrium. The details of the derivation can be found in Ref. [41] with respect to the set $\hat{\mathbf{B}}_\mathbf{i}$. The equation of motion for the thermodynamic set becomes

$$\frac{d}{dt}\begin{pmatrix}\hat{\mathbf{H}}\\ \hat{\mathbf{L}}\\ \hat{\mathbf{C}}\\ \hat{\mathbf{D}}\\ \hat{\mathbf{I}}\end{pmatrix}=\begin{pmatrix}-\Gamma & 0 & 0 & 0 & \Gamma E_{eq}\\ 0 & -\Gamma & -\Omega & 0 & 0\\ 0 & \Omega & -\Gamma & 0 & 0\\ \frac{2}{\hbar\Omega}\Gamma E_{eq} & 0 & 0 & -2\Gamma & 0\\ 0 & 0 & 0 & 0 & 0\end{pmatrix}\begin{pmatrix}\hat{\mathbf{H}}\\ \hat{\mathbf{L}}\\ \hat{\mathbf{C}}\\ \hat{\mathbf{D}}\\ \hat{\mathbf{I}}\end{pmatrix}, \tag{10}$$

where $\Gamma=\kappa^+ + \kappa^-$ and detailed balance requires $\kappa^+/\kappa^- = e^{-\hbar\Omega/k_BT}$. The equilibrium energy becomes $E_{eq}=\hbar\Omega(\kappa^+ - \kappa^-)/\Gamma = \hbar\Omega(e^{-2\hbar\Omega/k_BT}-1)/Z$, where $Z=1+2e^{-\hbar\Omega/k_BT}+e^{-2\hbar\Omega/k_BT}$. The temperature T is either T_c or T_h. Equation (10) factorizes; $\hat{\mathbf{H}}$ decouples from $\hat{\mathbf{L}}$ and $\hat{\mathbf{C}}$.

Equation (10) can be integrated leading to

$$\hat{\mathbf{H}}(t) = e^{-\Gamma t}[\hat{\mathbf{H}}(0) - E_{eq}\hat{\mathbf{I}}] + E_{eq}\hat{\mathbf{I}},$$

$$\hat{\mathbf{L}}(t) = e^{-\Gamma t}[\hat{\mathbf{L}}(0)\cos\,\Omega t - \hat{\mathbf{C}}(0)\sin\,\Omega t],$$

$$\hat{\mathbf{C}}(t) = e^{-\Gamma t}[\hat{\mathbf{C}}(0)\cos\,\Omega t + \hat{\mathbf{L}}(0)\sin\,\Omega t],$$

$$\hat{\mathbf{D}}(t) = \hat{\mathbf{D}}(0)e^{-2\Gamma t} + \frac{1}{\hbar\Omega}[\hat{\mathbf{H}}(0)E_{eq}(e^{-\Gamma t} - e^{-2\Gamma t}) - E_{eq}^2(e^{-\Gamma t}-1)\hat{\mathbf{I}}]. \tag{11}$$

From Eqs. (11) the propagators $\mathcal{U}_c$ and $\mathcal{U}_h$ can be constructed.

B. Dynamics on the magnetization and demagnetization *adiabats*

In general the dynamics on the demagnetization *adiabat* is generated by $\mathcal{L}=\mathcal{L}_H+\mathcal{L}_N$, where $\mathcal{L}_H=\frac{i}{\hbar}[\hat{\mathbf{H}},\cdot]$ and $\hat{\mathbf{H}}(t)$ is the time-dependent Hamiltonian [Eq. (4)]. The external noise generator $\mathcal{L}_N$ is defined and analyzed in Sec. IV. To follow the dynamics the equations of motions for the dynamical observables have to be solved. For the static set $\hat{\mathbf{B}}_1,\hat{\mathbf{B}}_2,\hat{\mathbf{B}}_3$ they become

$$\frac{d}{dt}\begin{pmatrix}\hat{\mathbf{B}}_1\\ \hat{\mathbf{B}}_2\\ \hat{\mathbf{B}}_3\end{pmatrix}(t)=\begin{pmatrix}0 & 0 & J\\ 0 & 0 & -\omega\\ -J & \omega & 0\end{pmatrix}\begin{pmatrix}\hat{\mathbf{B}}_1\\ \hat{\mathbf{B}}_2\\ \hat{\mathbf{B}}_3\end{pmatrix}, \tag{12}$$

and $\omega=\omega(t)$ is the time-dependent scheduling control function. More insight is obtained by shifting to the equation of motion for the time-dependent set $\hat{\mathbf{H}}$, $\hat{\mathbf{L}}$, and $\hat{\mathbf{C}}$. The solution is represented by the propagators $\mathcal{U}_{hc}$ and $\mathcal{U}_{ch}$. The integration to obtain $\mathcal{U}_{hc}$ and $\mathcal{U}_{ch}$ will be carried out with respect to a new time variable $d\Theta=\Omega dt$,

$$\frac{d}{\Omega dt}\begin{pmatrix}\hat{\mathbf{H}}\\ \hat{\mathbf{L}}\\ \hat{\mathbf{C}}\end{pmatrix}(t)=\begin{pmatrix}\frac{\dot{\Omega}}{\Omega^2} & -\frac{J\dot{\omega}}{\Omega^3} & 0\\ \frac{J\dot{\omega}}{\Omega^3} & \frac{\dot{\Omega}}{\Omega^2} & -1\\ 0 & 1 & \frac{\dot{\Omega}}{\Omega^2}\end{pmatrix}\begin{pmatrix}\hat{\mathbf{H}}\\ \hat{\mathbf{L}}\\ \hat{\mathbf{C}}\end{pmatrix}. \tag{13}$$

The ability of the working medium to follow the energy spectrum is defined by the adiabatic measure

$$\mu=\frac{J\dot{\omega}}{\Omega^3}. \tag{14}$$

We find that μ is a major parameter that characterizes the dynamics on the *adiabats*. When $\mu=0$ the propagator factorizes; the dynamics of $\hat{\mathbf{H}}$ is independent of the coupled pair $\hat{\mathbf{L}}$ and $\hat{\mathbf{C}}$. A large μ will cause large nonadiabatic changes coupling $\hat{\mathbf{H}}$ with $\hat{\mathbf{L}}$ and $\hat{\mathbf{C}}$ [Eqs. (13) and (18)]. In Appendix A, it is shown that constant μ minimizes the accumulated nonadiabatic transitions [defined in Eq. (19)].

Constant μ has the peculiarity that Eq. (13) can be integrated leading to a closed-form solution for the demagnetization and magnetization propagators $\mathcal{U}_{hc}$ and $\mathcal{U}_{ch}$. The consequence of stationary μ is a particular scheduling function of the external field $\omega(t)$ with time,

$$\omega(t)=\frac{Jf}{\sqrt{1-f^2}},\quad \Omega(t)=\frac{J}{\sqrt{1-f^2}}, \tag{15}$$

where $f(t)$ is a linear function of time: $f_{hc}(t)=\omega(t)/\Omega(t)=(t/\tau_{hc})(\omega_c/\Omega_c-\omega_h/\Omega_h)+\omega_h/\Omega_h$. Swapping h for c in $f(t)$ leads to the equivalent expression for the magnetization *adiabat*.

The adiabatic parameter and the time allocated to the *adiabat* obey the reciprocal relation

$$\mu_{hc}=\frac{K_{hc}}{\tau_{hc}}, \tag{16}$$

where $K_{hc}=\frac{1}{J}(\omega_c/\Omega_c-\omega_h/\Omega_h)$. Swapping c with h leads to μ_{ch} and then $K_{ch}=-K_{hc}$.

The solution is facilitated with the time variable Θ, $d\Theta=\Omega dt$. The final value of Θ_{hc} becomes $\Theta_{hc}=\tau_{hc}(1/K_{hc})\Phi_{hc}$, where $\Phi_{hc}=(\arcsin(\omega_c/\Omega_c)-\arcsin(\omega_h/\Omega_h))$ and $0>\Phi\geq-\frac{\pi}{2}$. Equation (13) is solved by noticing that the diagonal part is a unit matrix multiplied by a time-dependent scalar. Therefore, we seek a solution of the type $\mathcal{U}_{hc}=\mathcal{U}_1\mathcal{U}_2$, where $[\mathcal{U}_1,\mathcal{U}_2]=0$. The integral of the diagonal part of Eq. (13) becomes

$$\mathcal{U}_1=\exp\left(\int_0^{\tau_{hc}}\frac{\dot{\Omega}}{\Omega}dt\right)\hat{\mathbf{I}}=\frac{\Omega_c}{\Omega_h}\hat{\mathbf{I}}, \tag{17}$$

which can be interpreted as the scaling of the energy levels with the variation in Ω.

To integrate $\mathcal{U}_2$ the nondiagonal parts of Eq. (13) are diagonalized, leading to the eigenvalues $0,-i\sqrt{q},i\sqrt{q}$, where $q=\sqrt{1+\mu^2}$. Finally, the propagator becomes

$$\mathcal{U}_2 = \begin{pmatrix} \frac{1+\mu^2 c}{q^2} & -\frac{\mu s}{q} & \frac{\mu(1-c)}{q^2} \\ \frac{\mu s}{q} & c & -\frac{s}{q} \\ \frac{\mu(1-c)}{q^2} & \frac{s}{q} & \frac{\mu^2+c}{q^2} \end{pmatrix}, \tag{18}$$

where $s=\sin(q\Theta)$ and $c=\cos(q\Theta)$. The propagator $\mathcal{U}_2$ induces periodic mixing of $\hat{\mathbf{H}}$ with $\hat{\mathbf{L}}$ and $\hat{\mathbf{C}}$. As a result a diagonal $\hat{\boldsymbol{\rho}}_e$ [cf. Eq. (9)] will develop nondiagonal terms. To characterize the deviation from perfect factorization of $\hat{\mathbf{H}}$ from $\hat{\mathbf{L}}$ and $\hat{\mathbf{C}}$, we define an adiabaticity measure δ as

$$\delta = 1 - (\mathcal{U}_1^{-1})\mathcal{U}_{hc}(1,1), \tag{19}$$

where $\mathcal{U}_1^{-1}=(\Omega_h/\Omega_c)\hat{\mathbf{1}}$ is introduced to correct for the energy scaling. In the present context of noiseless dynamics and constant μ, $\delta=1-\mathcal{U}_2(1,1)$. When $\delta=0$ there is complete factorization. As will be described in Sec. V, $\delta\neq 0$ determines the minimum temperature.

The adiabatic limit is described by $\mu\to 0$. Then Eq. (18) converges to the identity operator. These are the perfect adiabatic following conditions where $\delta=0$. In general Eq. (18) describes a periodic motion of $\hat{\mathbf{H}}$, $\hat{\mathbf{L}}$, and $\hat{\mathbf{C}}$. Each period is defined by

$$q\Theta = 2\pi l, \quad l = 0,1,2,\ldots, \tag{20}$$

where l is the winding number. At the end of each period $\mathcal{U}_2$ restores to the identity matrix. These are the periodic frictionless conditions where $\delta=0$. For intermediate times $\langle\hat{\mathbf{H}}\rangle$ is always larger than the frictionless value $\delta>0$. The amplitude of this periodic dynamics decreases when μ becomes smaller [cf. $\mathcal{U}_2(1,1)$ in Eq. (18)]. Constant μ leads to the minimum of δ in Eq. (19) (cf. Appendix A).

The frictionless conditions define a quantization condition for the adiabatic parameter μ,

$$\mu = \left[\left(\frac{2\pi l}{\Phi_{hc}}\right)^2 - 1\right]^{-1/2}. \tag{21}$$

Examining Eq. (21) we find that there is no solution for $l=0$. The first frictionless solution is defined by $l\geq\sqrt{\Phi_{hc}/2\pi}$. This leads to a minimum demagnetization time [cf. Eq. (16)],

$$\tau_{hc}(\min) \geq K_{hc}\sqrt{\left(\frac{2\pi}{\Phi_{hc}}\right)^2 - 1}. \tag{22}$$

From Eq. (22) we can interpret that the minimal frictionless demagnetization time scales as $\tau_{hc}(\min)\propto\frac{1}{J}$ since it has a weak dependence on ω_c and ω_h. The special closed-form solution can be employed in a piecewise fashion to analyze other scheduling functions $\omega(t)$. In general we expect similar quantization of the solutions.

The main observation of this section is the existence of families of periodic frictionless solutions where the energy restores to its adiabatic value every period. Figure 1 shows frictionless magnetization and demagnetization *adiabats*. For $\mu\to 0$ these solutions coalesce with the adiabatic following solutions. Table I summarizes some of the notations used.

TABLE I. Notation and definitions.

Name	Notation	Comments
Compression ratio	$\mathcal{C}$	$\mathcal{C}=\frac{\Omega_h}{\Omega_c}$
Reversibility	$\mathcal{R}$	$\mathcal{R}=\frac{T_c\Omega_h}{T_h\Omega_c}$
Adiabatic measure	μ	$\mu=\frac{J\dot{\omega}}{\Omega^3}$
Reciprocal relation	$K=\tau\mu$	$K_{hc}=\frac{1}{J}(\frac{\omega_c}{\Omega_c}-\frac{\omega_h}{\Omega_h})$
Compression angle	Φ	$\Phi_{hc}=[\arcsin(\frac{\omega_c}{\Omega_c})-\arcsin(\frac{\omega_h}{\Omega_h})]$
Rotation angle	Θ	$\Theta=\frac{\Phi}{\mu}$
Heat conductivity	$\Gamma=\kappa^+ +\kappa_-$	$\frac{\kappa^+}{\kappa_-}=e^{-\hbar\Omega/k_BT}$
Adiabaticity	δ	$\delta=1-\mathcal{U}_1^{-1}\mathcal{U}_{hc}$
Phase noise	γ_p	$-\frac{\gamma_p}{\hbar^2}[\hat{\mathbf{H}},[\hat{\mathbf{H}},\hat{\mathbf{A}}]]$
Amplitude noise	γ_a	$-\gamma_a\omega^2[\hat{\mathbf{B}}_1,[\hat{\mathbf{B}}_1,\hat{\mathbf{A}}]]$

IV. INFLUENCE OF NOISE

Any realistic refrigerator is subject to noise on the external controls. The main point of this paper is that even an infinitesimal amount of noise will eliminate the frictionless solutions. The sensitivity to noise results from the requirement of precise control of the scheduling of the external field $\omega(t)$. To observe this effect requires an explicit quantitative model of the noise induced by the external controls.

First we consider a piecewise process controlling the scheduling of ω in time. At every time interval, ω is updated to its new value. For such a procedure random errors are expected in the duration of these time intervals described by the Liouville operator $\mathcal{L}_N$. We model these errors as a Gaussian delta correlated noise. This process is mathematically equivalent to a dephasing process on the demagnetization *adiabat* [43]. This stochastic dynamics can be modeled by a Gaussian semigroup with the generator [51,52],

$$\mathcal{L}_{N_p}(\hat{\mathbf{A}}) = -\frac{\gamma_p}{\hbar^2}[\hat{\mathbf{H}},[\hat{\mathbf{H}},\hat{\mathbf{A}}]], \tag{23}$$

which is termed phase noise. An equivalent dynamics to Eq. (23) is also obtained in the limit of weak quantum measurement of the instantaneous energy [53]. We seek a solution for the propagator of a product type $\mathcal{U}_a=\mathcal{U}_1\mathcal{U}_2\mathcal{U}_3$ where the equations of motion of $\mathcal{U}_3$ can be obtained from the interaction representation. The noiseless solution has $\mathcal{U}_3=\hat{\mathbf{1}}$. A closed-form expression has been derived in the limit of small μ. The details can be found in Appendix B. The approximate propagator $\mathcal{U}_3(\tau_{hc})$ for l revolutions becomes

$$\mathcal{U}_3(\tau_{hc}) \approx \begin{pmatrix} C & -S & 0 \\ S & C & 0 \\ 0 & 0 & 1 \end{pmatrix}, \tag{24}$$

where $S=\sin\alpha_l$ and $C=\cos\alpha_l$. The rotation angle α_l becomes

$$\alpha_l = -\pi\gamma_p J \ln\left(\frac{(\Omega_h+\omega_h)(\Omega_c-\omega_c)}{(\Omega_h-\omega_h)(\Omega_c+\omega_c)}\right). \tag{25}$$

It is important to notice that the asymptotic value of α_l is finite when $\mu\to 0$ [cf. Eq. (B8)]. For the quantization conditions when $\mathcal{U}_2=\hat{\mathbf{1}}$ the deviation of $\mathcal{U}_3$ from the identity operator defines δ. Asymptotically as $\mu\to 0$ and $\omega_c \ll J$,

$$\delta_{\min} = 1-\cos(\alpha_l) \approx \tfrac{1}{2}\pi^2\gamma_p^2 J^2 \ln^2(4\Omega_h/J). \tag{26}$$

A more obvious source of external noise is induced by fluctuations in the control frequency $\omega(t)$. Such a term represents Markovian random fluctuations in the externally controlled magnetic field. There will always be fluctuations which are fast compared to $2\pi/\Omega$. Such noise can be described by the Lindblad term

$$\mathcal{L}_{N_a}\hat{\mathbf{X}} = -\gamma_a\omega^2[\hat{\mathbf{B}}_1,[\hat{\mathbf{B}}_1,\hat{\mathbf{X}}]]. \tag{27}$$

The propagator $\mathcal{U}_3$ to lowest order in μ factorizes. The details can be found in Appendix B. Then the $\mathcal{U}_3(1,1)$ element decouples from the remaining part of the propagator and becomes

$$\mathcal{U}_3(1,1) = \exp\left[-\gamma_a J^2\int_0^{2\pi l} d\Theta\left(\frac{\omega^2(\Theta)}{\Omega^3(\Theta)}\right)\right]. \tag{28}$$

Equation (28) can be integrated and since $\mathcal{U}_2=\hat{\mathbf{1}}$ for an integer number of revolutions, then

$$\delta = 1-\mathcal{U}_3(1,1) \approx 1-e^{-\gamma_a(J^2\omega_h^2/3\Omega_h^2)\tau_{hc}}. \tag{29}$$

The smallest δ is achieved for a one period cycle [Eq. (22)], then $\delta_{\min}\approx\gamma_a J(\omega_h^2/\Omega_h^2)$.

The phase noise and the amplitude noise have a reciprocal relation with respect to l (cf. Fig. 11). Phase noise is minimized for large l and amplitude noise for small l. Another possible source of noise is caused by fluctuation in the interaction energy $\hat{\mathbf{H}}_{int}$. Analysis shows that such noise will lead to a similar expression to Eq. (29) where J^2 is replaced with ω_c^2. All these types of noise will lead to a minimum bath temperature the refrigerator can pump from [cf. Eq. (36)].

V. THERMODYNAMICAL RELATIONS

The maximal efficiency $\eta^{\max}$ of a heat engine is limited by the second law to the Carnot efficiency. For the quantum Otto-type cycle, the efficiency is limited by the ratio of the energy-level differences in the hot and cold sides for any spectrum that scales globally with Ω [41,44,54]. As a result we obtain the series of inequalities

$$\eta^{\max} = 1-\frac{\Omega_c}{\Omega_h} < 1-\frac{\omega_c}{\omega_h} < 1-\frac{T_c}{T_h}. \tag{30}$$

In the operation as a refrigerator the inequality in Eq. (30) is reversed. This imposes a restriction on the minimum cold bath temperature T_c,

$$T_c \geq \frac{\Omega_c}{\Omega_h}T_h, \tag{31}$$

where Ω_c is limited by J, and for the limit $\omega_h \gg J$ we obtain

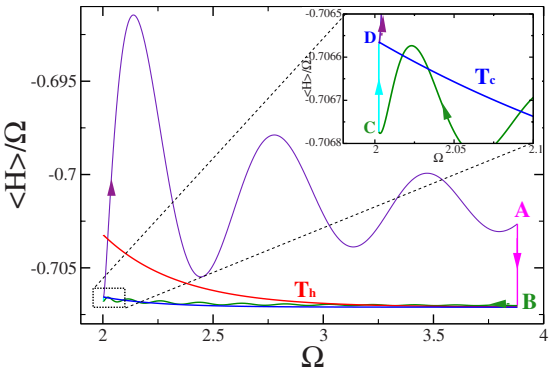

FIG. 2. (Color online) Typical optimal cycle of refrigerator with linear scheduling, in the $(\Omega,\langle\hat{\mathbf{H}}\rangle/\Omega)$ plane, eliminating the trivial propagation $\mathcal{U}_1$. The isotherms $\langle\hat{\mathbf{H}}\rangle_{eq}(T)$ corresponding to the cold and hot bath temperatures, T_c and T_h, are indicated. The cycle has the property $\langle\hat{\mathbf{H}}\rangle_C \leq \langle\hat{\mathbf{H}}\rangle_{eq}(T_c)$ (cf. insert). The cycle parameters are $J=2$, $T_c=0.18$, $T_h=0.24$, $\omega_c=0.1$, $\omega_h=3.325$, $\tau_c=12.292$, $\tau_h=11.615$, $\tau_{hc}=18.016$, and $\tau_{ch}=5.077$.

$$T_c \geq \frac{J}{\omega_h}T_h. \tag{32}$$

On the cold side the necessary condition for refrigeration is that the internal energy of the working medium at the end of the demagnetization is smaller than the equilibrium energy with the cold bath (cf. Fig. 2),

$$\langle\hat{\mathbf{H}}\rangle_C \leq \langle\hat{\mathbf{H}}\rangle_{eq}(T_c) = -\hbar\Omega_c(1-2e^{-\hbar\Omega_c/k_bT_c}), \tag{33}$$

where $\langle\hat{\mathbf{H}}\rangle_{eq}(T_c)$ is approximated by the low-temperature limit $\hbar\Omega_c \gg k_BT_c$. On the hot isochore the lowest-energy point B that can be obtained is in equilibrium with T_h: $\langle\hat{\mathbf{H}}\rangle_B \geq \langle\hat{\mathbf{H}}\rangle_{eq}(T_h) = -\hbar\Omega_h(1-2e^{-\hbar\Omega_h/k_bT_h})$. Under these conditions $L=C=0$. The change in $\langle\hat{\mathbf{H}}\rangle$ in the demagnetization *adiabat* leads to

$$\frac{\langle\hat{\mathbf{H}}\rangle_C}{\Omega_c} \approx (1-\delta)\frac{\langle\hat{\mathbf{H}}\rangle_B}{\Omega_h}, \tag{34}$$

where δ, the deviation from frictionless solutions, is defined in Eq. (19). Then the maximum heat that can be extracted per cycle becomes

$$\begin{aligned}\mathcal{Q}_c(\max) &= \langle\hat{\mathbf{H}}\rangle_{eq}(T_c) - \langle\hat{\mathbf{H}}\rangle_C \\ &\approx 2\hbar\Omega_c\left(e^{-\hbar\Omega_c/k_bT_c} - e^{-\hbar\Omega_h/k_bT_h} - \tfrac{1}{2}\delta\right).\end{aligned} \tag{35}$$

The condition for refrigeration is $\mathcal{Q}_c(\max)\geq 0$. When $\delta \ll e^{-\hbar\Omega_h/k_bT_h}$ the minimum temperature becomes the Carnot limit [Eq. (32)]. For sufficiently large ω_h, positive $\mathcal{Q}_c(\max) \geq 0$ leads to $\delta \leq 2e^{-\hbar\Omega_c/k_bT_c}$, imposing a stronger restriction on the minimal temperature,

$$T_c \geq \frac{\hbar J}{-k_B\ln(\delta/2)}. \tag{36}$$

Due to the logarithmic dependence on the noise δ the minimum temperature scales linearly with the uncontrolled part

of the energy gap $\hbar J$. Equation (36) relates the minimum temperature to δ, the adiabaticity parameter.

Power optimization

The cooling power $\mathcal{P}_c$ is the amount of heat extracted $\mathcal{Q}_c$ divided by the cycle time τ. For the frictionless solutions, the energy factorizes from the other variables; therefore, the heat extracted is obtained by considering the balance of heat and work required to close the cycle [38,44],

$$\mathcal{Q}_c = \hbar\Omega_c\left(\frac{E^h_{eq}}{\Omega_h} - \frac{E^c_{eq}}{\Omega_c}\right)\frac{(e^{x_c}-1)(e^{x_h}-1)}{1-e^{x_c+x_h}}$$
$$\approx 2\hbar\Omega_c(e^{-\hbar\Omega_h/k_bT_h} - e^{-\hbar\Omega_c/k_bT_c})F(x_c,x_h), \quad (37)$$

where $x_c=\Gamma_c\tau_c$ and $x_h=\Gamma_h\tau_h$. Optimizing the cooling power with respect to time allocation becomes equivalent to optimizing $F(x_c,x_h)/\tau_{cyc}$, where $\tau_{cyc}=\tau_h+\tau_{hc}+\tau_c+\tau_{ch}$ is the total cycle time. For frictionless solutions the minimum time on the *adiabats* τ_{hc} and τ_{ch} is described in Eq. (22). The optimal partitioning of the time allocation between the hot and cold *isochores* is obtained when

$$\Gamma_h[\cosh(\Gamma_c\tau_c)-1] = \Gamma_c[\cosh(\Gamma_h\tau_h)-1]. \quad (38)$$

When $\Gamma_h=\Gamma_c$ the optimal time allocations on the *isochores* becomes $\tau_h=\tau_c$. The total time allocation $\tau=\tau_{iso}+\tau_{adi}$ is partitioned to the time on the *adiabats* τ_{adi}, which is limited by the adiabatic condition, and the time τ_{iso} allocated to the *isochores*.

Optimizing the time allocation on the *isochores* subject to Eq. (38) leads to the optimal condition [44]

$$\Gamma_c\tau_{cyc}[\cosh(\Gamma_h\tau_h)-1] = \sinh(\Gamma_h\tau_h+\Gamma_c\tau_c) - \sinh(\Gamma_c\tau_c) - \sinh(\Gamma_h\tau_h). \quad (39)$$

When $\Gamma_h=\Gamma_c\equiv\Gamma$ this expression simplifies to

$$2x + \Gamma\tau_{adi} = 2\sinh(x) \quad (40)$$

(where $x=\Gamma_c\tau_c=\Gamma_h\tau_h$). For small x Eq. (40) can be solved leading to the optimal time allocation on the *isochores*: $\tau_c=\tau_h\approx(\Gamma\tau_{adi}/3)^{1/3}/\Gamma$. Taking into consideration the restriction on the adiabatic condition this time can be estimated to be $\tau_c=\tau_h\propto\frac{1}{\Gamma}(\frac{\Gamma}{J})^{1/3}$.

We can now expect two limits for the optimal cooling power; the first is when Γ is sufficiently large the cycle time τ_{cyc} will be dominated by the time on the *adiabats*, then for large ω_c (cf. Fig. 6),

$$\mathcal{P}_c(\max) \propto \hbar J^2 e^{-\hbar J/k_bT_c}. \quad (41)$$

When the heat transfer time dominates, $\tau_c > \tau_{hc}$ then

$$\mathcal{P}_c(\max) \propto \hbar\frac{J^{4/3}}{\Gamma^{2/3}}e^{-\hbar J/k_bT_c}. \quad (42)$$

Noise on the *adiabats* modifies the optimal time allocation. Phase noise has its minimum for large values of l [cf. Eq. (26)]. It approaches this minimum after a few revolutions independent of K_{hc}. The optimum power is a compromise between large time allocation on the *adiabat* to reach minimize noise and small cycle time to maximize power. As a result the scaling $\tau_{adi}\propto 1/J$ is still maintained; therefore, Eq. (41) or Eq. (42) will hold. For amplitude noise the minimum δ is obtained for the minimum time frictionless solution which also leads to the scaling of power as in Eq. (41).

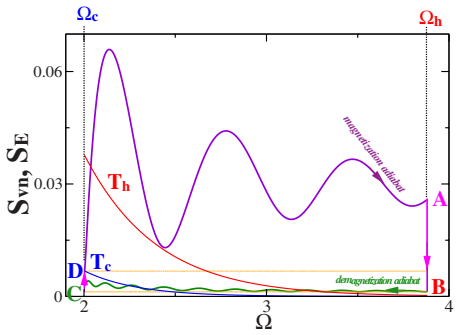

FIG. 3. (Color online) Typical optimal cycle of refrigerator with linear scheduling, with $T_c > T_c^{\min}$, in the (1) (Ω, S_E) and (2) (Ω, S_{VN}) planes (lower rectangle). The isotherms $\mathcal{S}_{eq}(T)$ corresponding to the cold and hot bath temperatures, T_c and T_h, are indicated. The difference between the energy entropy and the von Neumann entropy is the result of quantum friction: point A is higher than point D and point C is higher than point B. The cycle parameters are the same as in Fig. 2. $T_c(\min)\sim 0.1176$ from Fig. 6.

VI. SIMULATING THE CYCLE

After the segment propagators have been solved the cycle propagator can be assembled. For constant μ the cycle propagator $\mathcal{U}_{cyc}$ has a closed-form solution. Other scheduling functions $\omega(t)$ require numerical integration of the equation of motion [Eq. (13)]. We have verified that our numerical integration coincides with the analytical expressions when available.

The purpose of the simulation is to determine the optimal performance of the refrigerator. The cooling power was extracted from the limit cycle obtained by propagating the cycle iteratively from an initial state until convergence. The optimal cooling power was studied as a function of total cycle time τ. For a fixed cycle time the heat extracted $\mathcal{P}_c$ was optimized with respect to the time allocation on each segment. A random search procedure was used for this task.

In general two types of cycles emerge and are classified according to the cycle time. The first are sudden cycles with very short periods $\tau_{cyc}\ll\frac{2\pi}{\Omega}$ which are characterized by a global topology. These sudden cycles will be addressed separately [55]. The focus of the present study are cycles with a period comparable or longer than the internal time scale $\tau_{cyc}>2\pi/\Omega$. The cycles of optimal cooling rate and minimum temperature are of this type.

Figures 3 and 4 present a typical cycle constructed with $\omega(t)$ linear in t with optimal time allocation. Figure 3 displays the entropy frequency plane. Figure 4 shows the trajectory in the $\hat{\mathbf{H}}$, $\hat{\mathbf{L}}$, and $\hat{\mathbf{C}}$ coordinates. The positioning of the cycle with respect to the hot and cold isotherms shows that it operates as a refrigerator with positive $\mathcal{Q}_c$. The end point D of the cold isochore is below the equilibrium point

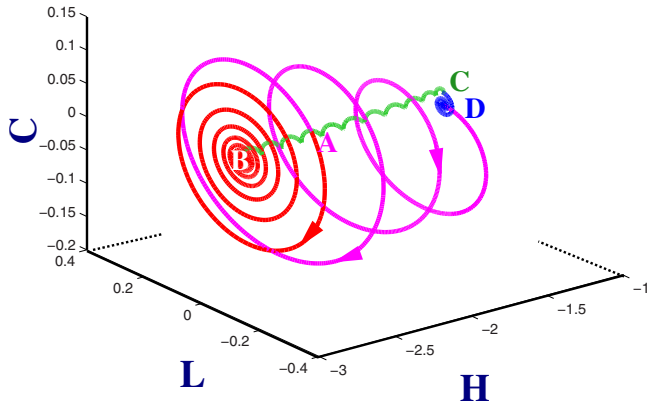

FIG. 4. (Color online) Typical optimal cycle trajectory with linear scheduling shown in the $\hat{\mathbf{H}}$, $\hat{\mathbf{L}}$, and $\hat{\mathbf{C}}$ coordinates, for the same parameters as in Fig. 3. Point A represents the beginning of the hot *isochore*. Point B represents the beginning of the demagnetization *adiabat*. Point C represents the beginning of the cold *isochore*. Point D represents the beginning of the magnetization *adiabat*. Notice the big difference between the demagnetization and magnetization *adiabats*.

with the cold bath. On the scale of Fig. 3 this is hard to observe. One should also notice that S_{VN}, which is constant on the *adiabats* and always a lower bound to S_E, almost touches the minimal S_E of the *adiabats*. The vertical distance from point D to point A and from point B to point C is the result of quantum friction.

The asymmetry between the demagnetization and magnetization *adiabats* can be noticed in both Figs. 3 and 4. The reason for this asymmetry is that the heat caused by friction in the magnetization *adiabat* can be dissipated to the hot bath. This is not true on the demagnetization *adiabat* where friction limits the possibility of heat extraction. This leads to very different time allocation $\tau_{hc} > \tau_{ch}$. The linear scheduling cycle should be compared to the cycles in Figs. 1 and 5 where the friction is limited due to the quantization. The obvious difference is the symmetry between the demagnetization and magnetization *adiabats*. At the beginning and the end of the frictionless segments the von Neumann and the energy entropies coincide. Periodic dynamics on the *adiabats*

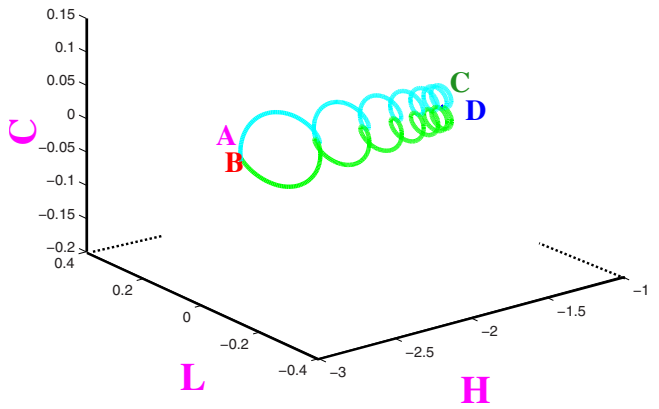

FIG. 5. (Color online) Typical optimal cycle trajectory shown in the $\hat{\mathbf{H}}$, $\hat{\mathbf{L}}$, and $\hat{\mathbf{C}}$ coordinates, corresponding to Fig. 1. Notice that on this scale the *isochores* are barely observable.

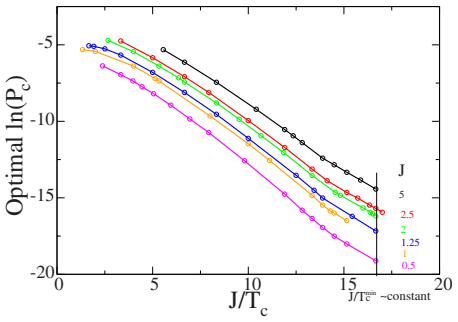

FIG. 6. (Color online) The logarithm of the optimal heat power $\mathcal{P}_c$ as a function of J/T_c for different J values (linear scheduling). On the graphs the ratio $\mathcal{R}=(T_c\Omega_h)/(T_h\Omega_c)=1.453$ is kept constant, where $\hbar\omega_c=0.1$ and $T_c/T_h=0.75$.

is also observed for optimal linear scheduling (cf. Fig. 4); nevertheless, frictionless solutions are not obtained.

Numerical experiments

We studied the optimal cooling cycles for a very large set of parameters for different scheduling functions. Figure 6 shows the optimal cooling power as a function of J/T_c, where the ratio $\mathcal{R}=T_c\Omega_h/T_h\Omega_c$ was maintained constant. The parameter $\mathcal{R}$ addresses the "distance" of the operation conditions from the reversible limit where $\mathcal{R}=1$. The simulations were performed for a predefined $\mathcal{R}>1$, so that the second law is never violated [cf. Eq. (32)]. Figure 6 was obtained for a linear scheduling function of $\omega(t)$ without the addition of noise. The feature is that all graphs for different J values terminate at the same minimum J/T_c. This graph has initiated our search for a possible explanation. In retrospect it represents the influence of uncontrolled numerical noise. Comparing to Eq. (36) we can estimate the value of δ as $\approx 10^{-7}$. In addition all lines corresponding to different J values can be collapsed by shifting vertically by $\ln J^2$. This finding shows consistency with the scaling of $\mathcal{P}_c$ with J^2 [cf. Eq. (41)].

Simulations with constant μ confirm the quantization behavior of the optimal conditions. Figure 7 displays $\mathcal{Q}_c$ for optimal cycles as a function of total cycle time τ. The quantization of the cycle time is apparent corresponding to almost frictionless complete revolutions on the *adiabats*. The comb-like function $\mathcal{Q}_c^{opt}(\tau)$ has a maximum at τ corresponding approximately to $l=8$ at the high temperature and $l=6$ at the lowest temperature, which is very close to the minimum temperature possible in these simulations. The maximum of $\mathcal{Q}_c^{opt}(\tau)$ is an indication of uncontrolled numerical noise in the simulation. Noiseless operation conditions would result in a flat comb distribution of $\mathcal{Q}_c^{opt}(\tau)$.

Figure 8 shows the entropy production as a function of cycle time. Only the cycles with very small entropy production corresponding to almost frictionless cycles, operate as refrigerators. All non quantized cycles have a very large entropy production which decreases when the cycle time becomes longer. The quantized cycle (insert) have a very small entropy production which increases with the cycle time τ. Figure 8 demonstrates that quantum friction is accompanied by large entropy production.

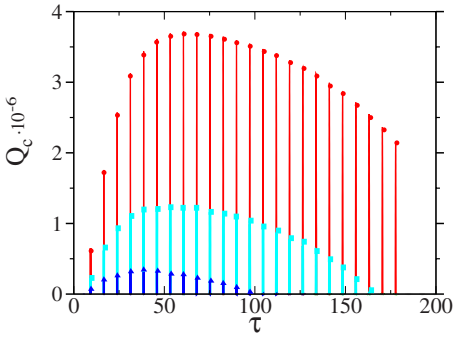

FIG. 7. (Color online) The optimal heat $\mathcal{Q}_C$ extracted as a function of cycle time for three sets of temperatures: $T_c=0.105$, $T_h=0.14$ (top: red circles); $T_c=0.0975$, $T_h=0.13$ (middle: cyan squares); and $T_c=0.09$, $T_h=0.12$ (bottom: blue triangles). Results obtained by random search for stationary μ with the restriction of $\tau_{hc}=\tau_{ch}$. Other parameters are $J=2$, $\hbar\omega_c=0.1$, $\hbar\omega_h=3.325\,76$, and no added noise.

We attempted to identify the character of the numerical noise in the simulation. The procedure was to estimate the minimum temperature for a set of parameters J, $\mathcal{R}$, and $\mathcal{C}=\Omega_c/\Omega_h$, the magnetization ratio. Then we used Eq. (35) to estimate δ. From the functional dependence of δ on the parameters we tried to empirically asses the numerical noise in the simulation. In general we found both phase and amplitude noise. This can be observed in the trimming of both the high and low l ends of the comb in Fig. 7. In general we found that δ is increased with $\mathcal{C}$, the compression ratio, and with $\mathcal{R}$, the deviation from reversibility. These dependencies were found for both constant μ and linear scheduling where the constant μ resulted consistently with a lower minimum temperature. The findings indicate that there is an additional source of numerical noise beyond the amplitude and phase noise.

The existence of uncontrolled numerical noise hinders the study of the additional effects of the imposed phase and amplitude noise. The cycle simulation was repeated with the addition of phase noise [cf. Eq. (B1)]. As can be seen in Fig. 9 an increasing amount of phase noise depresses $\mathcal{Q}_c$ and moves the maximum to larger τ_{cyc} or larger l [cf. Eq. (B7) and text after]. Numerical noise trims the high values of l.

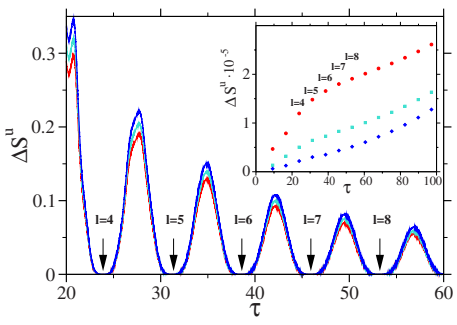

FIG. 8. (Color online) The entropy production $\Delta\mathcal{S}^u$ as a function of cycle time for three sets of temperatures corresponding to Fig. 7. Only the cycles with almost zero $\Delta\mathcal{S}^u$ function as refrigerators. Their entropy production is shown in the inset on a very different scale. The quantum numbers are indicated. The break in the slope corresponds to the maximum $\mathcal{P}_c$ in Fig. 7.

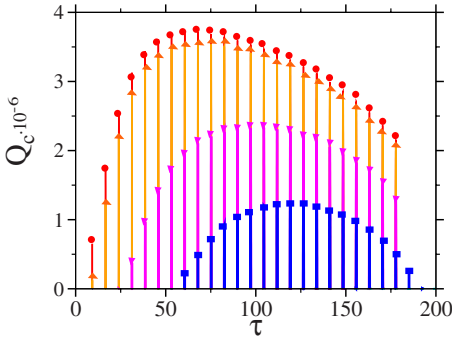

FIG. 9. (Color online) The optimal heat $\mathcal{Q}_C$ extracted as a function of cycle time for three values of external phase noise γ_p: top (red circles): $\gamma_p=0$, middle (orange triangles pointing up): $\gamma_p=10^{-6}$, middle (magenta triangles pointing down): $\gamma_p=10^{-5}$, and bottom (blue squares): $\gamma_p=2\times10^{-5}$. $\gamma_p=5\times10^{-5}$ did not result in positive $\mathcal{Q}_c$. Other parameters are as in Fig. 7.

The quantization of the optimal cycles is independent of the specific scheduling. When the cold bath temperature T_c is increased the quantization of $\mathcal{Q}_c$ and $\mathcal{P}_c$ is less pronounced. This can be seen in Fig. 10 where the optimal power is plotted as a function of cycle time τ for linear scheduling. The sharp comb structures in Fig. 7 are replaced with periodic modulation on top of a continuous background. At higher temperatures cycle with more friction can still operate as a refrigerator. Then the quantization features are washed out.

VII. SUMMARY

A reciprocating quantum refrigerator is more than the product of its four segments. To operate, the refrigerator has to complete the cycle. This limit cycle is then invariant to the global four-stroke propagator $\mathcal{U}_{cyc}$. Optimizing the performance becomes an interplay between optimizing the segments and their global synergism. In the analysis the unifying element was the vector space of thermodynamical observables. This vector space is sufficient to uniquely define the state of the system $\hat{\boldsymbol{\rho}}$. A central part of the study was devoted to generate the segment propagators which operate

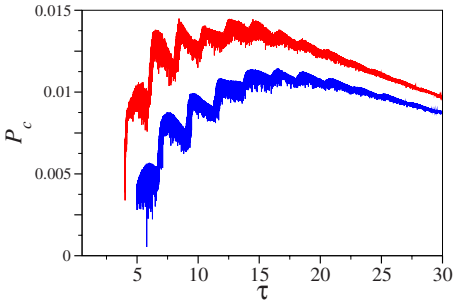

FIG. 10. (Color online) The optimal cooling power $\mathcal{P}_C$ as a function of cycle time for linear scheduling. Upper plot (red): $\hbar\omega_c=0.5$ and $\hbar\omega_h=3.9$. Lower plot (blue): $\hbar\omega_c=0.1$, $\hbar\omega_h=3.4$. $\hbar J=1.25$, $T_c=0.725$, and $T_h=0.966$.

on the closed set of these observables. We have found analytical expressions for all segments. This has allowed a thorough investigation of the refrigerator's properties.

The dynamics on the isomagnetic *isochores* represent a monotonic approach to thermal equilibrium [cf. Eq. (10)]. The equations simplify due to factorization of the vector space [cf. Eq. (11)]. This in turn reflects on the demagnetization *adiabats* which have to supply initial states with energy below the cold equilibrium point. Optimization with respect to cooling power requires one to stop the equilibration process before actually reaching thermal equilibrium. The time allocated depends again on the time allocated to the adiabatic segments, which is required to reduce friction [cf. Eq. (39)].

Quantum friction is the result of the inability of the system to follow adiabatically the time-dependent changes in the Hamiltonian $[\hat{\mathbf{H}}(t),\hat{\mathbf{H}}(t')]\neq 0$. As a result the state of the system will develop nondiagonal terms in the energy representation $\hat{\boldsymbol{\rho}}_e$. The signature of this phenomena is an increase in the energy entropy $\mathcal{S}_E$. The key to cold temperature refrigeration is frictionless dynamics: no increase in energy in the demagnetization segment beyond the adiabatic limit. Perfect adiabatic following which requires infinite time will lead to frictionless demagnetization. Under conditions that fulfill the second law $\mathcal{R}>1$, the cooling can continue to $T_c=0$; the absolute zero is attainable. We then introduced an adiabatic measure μ to characterize the instantaneous nonadiabatic coupling. The limit $\mu\to 0$ corresponds to perfect adiabatic following. Our first surprise was that constant μ led to closed-form solutions for the dynamics. Moreover, these solutions unraveled a quantized family of frictionless solutions $\delta=0$. These solutions are characterized by a state $\hat{\boldsymbol{\rho}}$ commuting with the Hamiltonian at the beginning and end of the segment $[\hat{\mathbf{H}}(0),\hat{\boldsymbol{\rho}}_B]=[\hat{\mathbf{H}}(\tau_{hc}),\hat{\boldsymbol{\rho}}_C]=0$. The frictionless propagator is unitary. Any attempt to observe the energy before the end of the segment will destroy this unitary property and lead to friction. This is similar to quantum gates which have the property that observing them during execution will destroy the gate. A weak continuous measurement is equivalent to phase noise and also destroys the unitary property. Similar frictionless solutions were found for a working medium constructed from harmonic oscillators [46,47]. This frictionless solution can be carried out in a finite cycle time, i.e., the cooling power does not vanish, $\mathcal{P}_c>0$. If these frictionless cycles could be realized they could operate to $T_c=0$.

When attempting to simulate numerically the frictionless cycles we got into conflict. Any attempt resulted in a minimum temperature $T_c(\min)$ which scaled linearly with the minimal energy gap $\hbar J$. This observation eventually led us to the realization that any cycle is subject to noise. To follow this idea we constructed a model for the external noise on the controls. Amplitude noise is the result of fluctuations in the magnitude of the external magnetic field. Since this noise term does not commute with the Hamiltonian, it is not surprising that it will destroy the adiabaticity, leading to $\delta>0$. The surprise was the devastating effect of phase noise which commutes with the instantaneous Hamiltonian. Such a term can be the result of weak continuous measurement of energy on the *adiabats*. This type of measurement leads to partial collapse of the state to the energy representation. Naively one would expect this to lead to frictionless solutions [22]. We have employed such an idea successfully to reduce friction in a quantum engine [43]. Nevertheless, for a refrigeration cycle close to its minimum temperature phase noise accumulates leading to $\delta>0$. Both types of noise are sufficient to eliminate frictionless solutions including the perfect infinite time adiabatic following frictionless cycle.

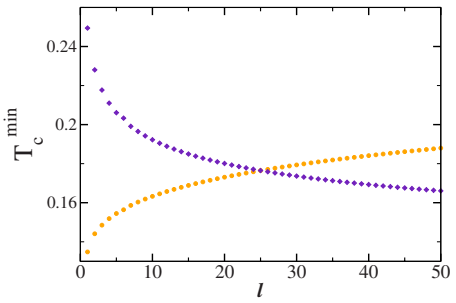

FIG. 11. (Color online) The minimum temperature as a function of the quantization number l. The diamonds represent phase noise and the circles represent amplitude noise; $\hbar J=2$.

Once the devastating effect of noise is appreciated it can be directly linked to a restriction on the minimum temperature. The minimum temperature $T_c^{\min}$ depends on $-1/\ln\delta$ [cf. Eq. (36)] and will be on the order of the uncontrolled energy gap $\hbar J$. This finding is consistent with experiments on demagnetization cooling of a gas [56] which obtained a minimum temperature an order of magnitude larger than the theoretical prediction [57], attributing the discrepancy to noise in the controls. Figure 11 shows the dependence of the minimum temperature of a refrigerator subject to phase and amplitude noise. The minimum temperature is related to the quantum number l of the frictionless solutions. The two types of noise show an opposite dependence on l. Amplitude noise favors small cycle times $l=1$ while phase noise favors small μ, meaning large l or τ. When both types of noise are simultaneously present the minimum temperature will be influenced by both in an intermediate l (cf. Fig. 11). Other sources of noise will also limit $T_c(\min)$; for example, our study was hindered by numerical noise.

To conclude, it seems that any refrigerator constructed with a working medium possessing an uncontrolled energy gap will reach a minimum operating temperature on the order of the minimum energy gap, i.e., the absolute zero is unattainable for a refrigerator subject to noise. This conjecture should be verified for refrigerators with gapless working media.

ACKNOWLEDGMENTS

We want to thank Yair Rezek, Peter Salamon, and Lajos Diósi for crucial discussions. This work was supported by the Israel Science Foundation.

APPENDIX A: OPTIMALITY OF CONSTANT μ

We show that for dynamics under the Hamiltonian (4) constant μ is the minimum of the nonadiabatic deviations,

i.e., minimum of δ. We can transform Eq. (14) to the differential equality, $\mu dt = d\omega/\Omega^3$, leading to

$$\int_0^{\tau_{hc}} \mu(t)dt = \int_{\omega_h}^{\omega_c} \frac{d\omega}{\Omega^3}. \tag{A1}$$

We decompose μ to a constant and a time-dependent part $\mu = \mu_0 + \mu_1 g(t)$. Without loss of generality we impose $\mu_0 \tau_{hc} = \int_{\omega_h}^{\omega_c} d\omega/\Omega^3$, then $\int_0^{\tau_{hc}} g(t)dt = 0$.

The first-order correction to the propagator $\mathcal{U}_2$ due to time dependence in μ is the time average $(1/\tau_{hc})\int_0^{\tau_{hc}} dt \mathcal{U}_2(t)$. This will translate to a time average of δ. The dependence of δ [Eqs. (19) and (18)] on μ is

$$\delta = \mu^2 \frac{(1-c)}{1+\mu^2}, \tag{A2}$$

which is a monotonic increasing function of μ^2 with minimum at $\mu^2 = 0$. The first-order correction to $\mathcal{U}_2$ will lead to $\delta = \delta_0 + \delta_1$, where δ_0 is the stationary result. Then expanding in μ_1 will lead to $\delta_1 = [(1-c)/(1+\mu_0^2)](\mu_1^2/\tau_{hc})\int_0^{\tau_{hc}} g^2(t)dt$ which is positive definite; therefore, a stationary μ is a minimum of δ.

APPENDIX B: DERIVATION OF THE NOISY PROPAGATOR $\mathcal{U}_3$

For the phase noise the dissipative generator is $\mathcal{L}_{N_p}(\hat{\mathbf{A}}) = -(\gamma_p/\hbar^2)[\hat{\mathbf{H}},[\hat{\mathbf{H}},\hat{\mathbf{A}}]]$ [Eq. (23)]. The modified equations of motion on the *adiabats* become

$$\frac{d}{\Omega dt}\begin{pmatrix}\hat{\mathbf{H}}\\ \hat{\mathbf{L}}\\ \hat{\mathbf{C}}\end{pmatrix}(t) = \begin{pmatrix} \frac{\dot{\Omega}}{\Omega^2} & -\frac{J\dot{\omega}}{\Omega^3} & 0 \\ \frac{J\dot{\omega}}{\Omega^3} & \frac{\dot{\Omega}}{\Omega^2} - \gamma_p\Omega & -1 \\ 0 & 1 & \frac{\dot{\Omega}}{\Omega^2} - \gamma_p\Omega \end{pmatrix}\begin{pmatrix}\hat{\mathbf{H}}\\ \hat{\mathbf{L}}\\ \hat{\mathbf{C}}\end{pmatrix}. \tag{B1}$$

We seek a solution of the product form $\mathcal{U}_a = \mathcal{U}_1\mathcal{U}_2\mathcal{U}_3$. The equations of motion of $\mathcal{U}_3$ are obtained from the interaction representation,

$$\begin{aligned}\frac{d}{\Omega dt}\mathcal{U}_3(t) &= \mathcal{U}_2(-t)\begin{pmatrix}0 & 0 & 0\\ 0 & -\gamma_p\Omega & 0\\ 0 & 0 & -\gamma_p\Omega\end{pmatrix}\mathcal{U}_2(t)\mathcal{U}_3(t)\\ &= \mathcal{W}(t)\mathcal{U}_3(t),\end{aligned} \tag{B2}$$

where

$$\mathcal{W}(t) = \gamma_p\Omega(t)\begin{pmatrix} \frac{\mu^2}{q^4}[s^2\mu^2 + 2(1-c)] & \frac{\mu s}{q^3}(\mu^2 c + 1) & -\frac{\mu}{q^4}(1-c)(\mu^2 c + 1) \\ \frac{\mu s}{q^3}(\mu^2 c + 1) & \frac{\mu^2 c^2 + 1}{q^2} & \frac{\mu^2 s}{q^3}(1-c) \\ -\frac{\mu}{q^4}(1-c)(\mu^2 c + 1) & \frac{\mu^2 s}{q^3}(1-c) & 1 - \frac{\mu^2}{q^4}(1-c)^2 \end{pmatrix}. \tag{B3}$$

$\mathcal{U}_3$ describes the dynamics with respect to the reference provided by the unitary trajectory $\mathcal{U}_2$. We seek an approximate solution for $\mathcal{U}_3$ in the limit when $\mu \to 0$, then $\mathcal{U}_2 = \hat{\mathbf{1}}$ since this is the frictionless limit. Expanding Eq. (B3) to first order in μ leads to

$$\mathcal{W}(t) \approx \gamma_p\Omega(t)\begin{pmatrix} 0 & \mu s & \mu(1-c) \\ \mu s & 1 & 0 \\ \mu(1-c) & 0 & 1 \end{pmatrix}. \tag{B4}$$

$\mathcal{U}_3(\tau_{hc})$ is solved in two steps. First is evaluating the propagator for one period of Θ, for which $\Omega(t)$ is almost constant, and then the global propagator becomes the product of the one period propagators for l periods: $\mathcal{U}_3(\tau_{hc}) \approx \mathcal{U}_3(\Theta = 2\pi)^l$. The Magnus expansion [58] to second order is employed to obtain the one period propagator $\mathcal{U}_3(2\pi)$,

$$\mathcal{U}_3(\Theta = 2\pi) \approx e^{\mathcal{M}_1 + \mathcal{M}_2 + \cdots}, \tag{B5}$$

where $\mathcal{M}_1 = \int_0^{2\pi} d\Theta \mathcal{W}(\Theta)$ and $\mathcal{M}_2 = \frac{1}{2}\int_0^{2\pi}\int_0^{\Theta} d\Theta d\Theta' \times [\mathcal{W}(\Theta), \mathcal{W}(\Theta')] + \cdots$. The first-order Magnus term leads to

$$\begin{aligned}&\mathcal{U}_3(\Theta = 2\pi)_{M_1}\\ &\approx \begin{pmatrix} 1 & 0 & \mu(1 - e^{-2\pi\gamma_p\Omega}) \\ 0 & e^{-2\pi\gamma_p\Omega} & 0 \\ \mu(1 - e^{-2\pi\gamma_p\Omega}) & 0 & e^{-2\pi\gamma_p\Omega} \end{pmatrix},\end{aligned} \tag{B6}$$

which to first order in μ, δ remains zero. $\mathcal{U}_3$ does not couple $\langle\hat{\mathbf{H}}\rangle$ with $\langle\hat{\mathbf{L}}\rangle$ and $\langle\hat{\mathbf{C}}\rangle$.

The second-order Magnus approximation leads to a structure of a rotation matrix,

$$\mathcal{U}_3(\Theta=2\pi)_{M_2} \approx \begin{pmatrix} C & -S & 0 \\ S & C & 0 \\ 0 & 0 & 1 \end{pmatrix}, \tag{B7}$$

where $S=\sin\alpha$ and $C=\cos\alpha$. $\alpha=\gamma_p\Omega\pi\mu\sqrt{9\mu^2+4}$ and as $\mu^2 \ll \frac{4}{9}$, $\alpha=2\gamma_p\Omega\pi\mu$. The term can be approximated as $\alpha \approx \Phi_{hc}\gamma_p\Omega\frac{1}{l}$ [cf. Eq. (21)]. The condition $\mu^2 \ll \frac{4}{9}$ can be transformed to $l \gg \frac{9\Phi}{8\pi}$. An *adiabat* with a small number of revolutions $l \approx 10$ already fulfills this condition. We now combine the second-order propagator $\mathcal{U}_3(\tau_{hc})$, for l revolutions. It has also the structure of a rotation matrix identical to Eq. (B7), with a new rotation angle $\alpha=\alpha_l$, where

$$\alpha_l = 2\pi\gamma_p\mu\int_0^{2\pi l}\Omega(\Theta)d\Theta = -\pi\gamma_p J\ln\left[\frac{(\Omega_h+\omega_h)(\Omega_c-\omega_c)}{(\Omega_h-\omega_h)(\Omega_c+\omega_c)}\right]. \tag{B8}$$

For the amplitude noise the dissipative generator is $\mathcal{L}_{N_a}(\hat{\mathbf{A}})=-\gamma_a\omega^2[\hat{\mathbf{B}}_1,[\hat{\mathbf{B}}_1,\hat{\mathbf{A}}]]$ [Eq. (27)]. In analogy to Eqs. (23) and (B2) the equation for $\mathcal{U}_3$ becomes

$$\frac{d}{\Omega dt}\mathcal{U}_3(t) = -\gamma_a\frac{\omega^2}{\Omega}\mathcal{U}_2(-t)\begin{pmatrix} \frac{J^2}{\Omega^2} & \frac{J\omega}{\Omega^2} & 0 \\ \frac{J\omega}{\Omega^2} & \frac{\omega^2}{\Omega^2} & 0 \\ 0 & 0 & 1 \end{pmatrix}\mathcal{U}_2(t)\mathcal{U}_3(t) = \mathcal{W}(t)\mathcal{U}_3(t). \tag{B9}$$

We seek an approximate solution for the quasistatic limit when $\mu \to 0$. Expanding $\mathcal{W}$ in Eq. (B9) to zero order in μ leads to

$$\mathcal{W}(\Theta) \approx -\gamma_a\frac{\omega^2}{\Omega^3}\begin{pmatrix} J^2 & J\omega c & -J\omega s \\ J\omega c & \omega^2+s^2J^2 & scJ^2 \\ -J\omega s & scJ^2 & J^2c^2+\omega^2 \end{pmatrix}. \tag{B10}$$

Since in this limit $c \to 0$ as $\mu \to 0$, then Eq. (B10) factorizes. We calculate the propagator for an integer number of periods; the lowest-order Magnus expansion becomes $\mathcal{U}_3(\Theta=2\pi l)=\exp(\int_0^{2\pi l}d\Theta\mathcal{W}(\Theta))$, then the $\mathcal{U}_3(1,1)$ element decouples from the remaining part of the propagator and becomes Eq. (28).

[1] J. Geusic, E. S. du Bois, R. D. Grasse, and H. Scovil, Phys. Rev. **156**, 343 (1967).
[2] R. Kosloff, J. Chem. Phys. **80**, 1625 (1984).
[3] Eitan Geva and Ronnie Kosloff, J. Chem. Phys. **104**, 7681 (1996).
[4] Ronnie Kosloff, Eitan Geva, and Jeffrey M. Gordon, J. Appl. Phys. **87**, 8093 (2000).
[5] José P. Palao, Ronnie Kosloff, and Jeffrey M. Gordon, Phys. Rev. E **64**, 056130 (2001).
[6] S. Lloyd, Phys. Rev. A **56**, 3374 (1997).
[7] J. He, J. Chen, and B. Hua, Phys. Rev. E **65**, 036145 (2002).
[8] C. M. Bender, D. C. Brody, and B. K. Meister, Proc. R. Soc. London, Ser. A **458**, 1519 (2002).
[9] T. D. Kieu, Phys. Rev. Lett. **93**, 140403 (2004).
[10] A. E. Allahverdyan, R. Balian, and Th. M. Nieuwenhuizen, EPL **67**, 565 (2004).
[11] D. Segal and A. Nitzan, Phys. Rev. E **73**, 026109 (2006).
[12] P. Bushev, D. Rotter, A. Wilson, F. Dubin, C. Becher, J. Eschner, R. Blatt, V. Steixner, P. Rabl, and P. Zoller, Phys. Rev. Lett. **96**, 043003 (2006).
[13] Dominik Janzing, J. Stat. Phys. **122**, 531 (2006).
[14] E. Boukobza and D. J. Tannor, Phys. Rev. Lett. **98**, 240601 (2007).
[15] E. Boukobza and D. J. Tannor, Phys. Rev. A **78**, 013825 (2008).
[16] J. Birjukov, T. Jahnke, and G. Mahler, Eur. Phys. J. B **64**, 105 (2008).
[17] T. Jahnke, J. Birjukov, and G. Mahler, Annal. Phys. **17**, 88 (2008).
[18] A. E. Allahverdyan, R. S. Johal, and G. Mahler, Phys. Rev. E **77**, 041118 (2008).
[19] D. Segal, J. Chem. Phys. **130**, 134510 (2009).
[20] H. Wang, S. Q. Liu, and J. Z. He, Phys. Rev. E **79**, 041113 (2009).
[21] He JiZhou, He Xian, and Tang Wei, Sci. China, Ser. G **52**, 1317 (2009).
[22] J. Gemmer, M. Michel, and G. Mahler, *Quantum Thermodynamics* (Springer, New York, 2009).
[23] W. Nernst, Nachr. Kgl. Ges. Wiss. Goettingen **40** (1906).
[24] W. Nernst, Ber. Kgl. Ges. Wiss. Goettingen **40** (1906).
[25] W. Nernst, *The Theoretical and Experimental Bases of the New Heat Theorem* (W. Knapp, Halle, 1918), German translation is *Die Theoretischen und Experimentellen Grundlagen des Neuen Warmesatzes*.
[26] P. T. Landsberg, Rev. Mod. Phys. **28**, 363 (1956).
[27] F. Belgiorno, J. Phys. A **36**, 8165 (2003).
[28] F. Belgiorno, J. Phys. A **36**, 8195 (2003).
[29] A. S. Oja and O. V. Lounasmaa, Rev. Mod. Phys. **69**, 1 (1997).
[30] N. Kurti, Physica B & C **109-110**, 1737 (1982).
[31] P. Hakonen, O. V. Lounasmaa, and A. Oja, J. Magn. Magn. Mater. **100**, 394 (1991).
[32] Feng Wu, Lingen Chen, Shuang Wu, and Fengrui Sun, J. Phys. D: Appl. Phys. **39**, 4731 (2006).
[33] K. A. Gschneider, Jr., V. K. Pecharsky, and A. O. Tsokol, Rep. Prog. Phys. **68**, 1479 (2005).
[34] A. Rowe and A. Tura, Int. J. Refrig. **29**, 1286 (2006).
[35] Tova Feldmann and Ronnie Kosloff, EPL **89**, 20004 (2010).
[36] Eitan Geva and Ronnie Kosloff, J. Chem. Phys. **96**, 3054 (1992).
[37] Eitan Geva and Ronnie Kosloff, J. Chem. Phys. **97**, 4398 (1992).
[38] Tova Feldmann, Eitan Geva, Ronnie Kosloff, and Peter Sala-

mon, Am. J. Phys. **64**, 485 (1996).
[39] Tova Feldmann and Ronnie Kosloff, Phys. Rev. E **61**, 4774 (2000).
[40] Ronnie Kosloff and Tova Feldmann, Phys. Rev. E **65**, 055102 (2002).
[41] Tova Feldmann and Ronnie Kosloff, Phys. Rev. E **68**, 016101 (2003).
[42] Tova Feldmann and Ronnie Kosloff, Phys. Rev. E **70**, 046110 (2004).
[43] Tova Feldmann and Ronnie Kosloff, Phys. Rev. E **73**, 025107(R) (2006).
[44] Yair Rezek and Ronnie Kosloff, New J. Phys. **8**, 83 (2006).
[45] P. Salamon, J. D. Nulton, G. Siragusa, T. R. Andersen, and A. Limon, Energy **26**, 307 (2001).
[46] Peter Salamon, Karl Heinz Hoffmann, Yair Rezek, and Ronnie Kosloff, Phys. Chem. Chem. Phys. **11**, 1027 (2009).
[47] Yair Rezek, Peter Salamon, Karl Heinz Hoffmann, and Ronnie Kosloff, EPL **85**, 30008 (2009).
[48] Xi Chen, A. Ruschhaupt, S. Schmidt, A. del Campo, D. Guery-Odelin, and J. G. Muga, Phys. Rev. Lett. **104**, 063002 (2010).
[49] G. Lindblad, Commun. Math. Phys. **48**, 119 (1976).
[50] R. Alicki and K. Lendi, *Quantum Dynamical Semigroups and Applications* (Springer-Verlag, Berlin, 1987).
[51] H.-P. Breuer and F. Petruccione, *Open Quantum Systems* (Oxford University Press, New York, 2002).
[52] V. Gorini and A. Kossakowski, J. Math. Phys. **17**, 1298 (1976).
[53] L. Dio'si, in *Encyclopedia of Mathematical Physics*, edited by J.-P. Fransoise, G. L. Naber, and S. T. Tsou (Elsevier, Oxford, 2006), Vol. 4, p. 276.
[54] F. Rempp, M. Michel, and G. Mahler, Phys. Rev. A **76**, 032325 (2007).
[55] T. Feldmann and R. Kosloff (unpublished).
[56] M. Fattori, T. Koch, S. Goetz, A. Griesmair, S. Hensler, J. Stuhler, and T. Pfau, Nat. Phys. **2**, 765 (2006).
[57] S. Hensler, A. Greiner, J. Stuhler, and T. Pfau, EPL **71**, 918 (2005).
[58] S. Blanes, F. Casas, J. A. Oteo, and J. Ros, Phys. Rep. **470**, 151 (2009).